MULTIPLE EQUILIBRIUM STATES DURING THE QUASI-STEADY FORMATION OF BUBBLES AND DROPS AT A CIRCULAR ORIFICE

Sanda-Carmen GEORGESCU[1], Jean-Luc ACHARD[2]

Instabilities occurring during the quasi-steady formation of bubbles and drops at a submerged orifice, under constant pressure conditions, have been investigated numerically. For different values of the control parameters of the problem, namely the Eötvös number Eö, and the excess pressure number Δ, which denotes the pressure difference between gas and liquid across the orifice, computed interface profiles are characterized by the apex height h, positive for bubbles, and negative for drops. At high apex height values, bubbles and drops have an undulate structure, with one or two necks. In the three-dimensional space (Eö,Δ,h), the equilibrium surface is multifold in both Δ directions, and some singularity lines intersect to form higher singularities. The central singularity is a cusp that straddles on the flat meniscus, between emerging bubbles and pendant drops profiles. The upper cusp sheet corresponds to bubbles, and the lower one corresponds to drops. Several fold curves that correspond to the multifold surface delimit stable and unstable regions. The first four fold curves are roughly parallel, while the following-ones are distorted, and exhibit a sequence of swallowtails. The numerical bifurcation set is computed onto the control parameter plane (Eö,Δ), extending in particular the analytical bifurcation set that is valid only around the critical point, defined at Eö = 5.783186, $\Delta = 0$, *and* $h = 0$.

Keywords: bubble/drop formation, meniscus stability, cusp, swallowtail

1. Introduction

To enhance the transport rate between gaseous and liquid phases, many engineering applications involve formation of gas bubbles and liquid drops. We focus here on the quasi-steady formation of bubbles and drops at a submerged orifice [1; 2]. Experimental evidence on Newtonian fluids shows that, usually, stable bubbles and drops, which form without phase change, have not an undulate structure. However, Padday [3] studied the bifurcation and breakage of a pendant drop, using an ultra high-speed cine camera. Some of its frames, especially those with satellite drop formation, are reminiscent of drop configurations that may be

[1] Assoc. Prof., PhD, Hydraulics, Hydraulic Machinery & Env. Protection Dept, Power Engineering Faculty, University POLITEHNICA of Bucharest, Romania, e-mail: carmen.georgescu@upb.ro
[2] CNRS Res. Dir. PhD, Laboratory of Geophysical and Industrial Flows (LEGI), Grenoble, France

considered as necked. Chains of bubbles connected by thin necks have been observed by Kliakhandler [4], but only in concentrated polymeric solutions, where bubbles may form a very stable, continuous, and slowly rising *bubbles sausage*. The elastic properties of the liquid prevent the collapse of necks, and detachment of rising bubbles from each other. The same author conducted additional experiments with bubbling in viscous Newtonian liquids (corn syrup, silicon oil), but no undulate bubble structure could be formed. In experimental studies about the dynamics associated with a single bubble during nucleate boiling on a horizontal surface, necked bubble profiles have been observed by Pakleza *et al*. [5]: vapour bubbles could not be stabilised, but their growth is low enough to meet temporarily some undulate steady configurations during their life. Note that, in this experiment, the saturated vapour pressure is controlled via the temperature.

We limit our interest to processes without phase change, and select systems that contain Newtonian fluids. Each particle (bubble, drop) interface is attached to the edge of a circular orifice through a thin plate, which separates an upper cylindrical vessel of quiescent liquid, from a lower air chamber maintained at constant pressure. Thus, the quasi-steady formation of bubbles and drops appears as a process mainly governed by a balance of interfacial tension and gravity forces. The analysis performed analytically by Achard and Georgescu [6] has brought a unified picture of the quasi-steady formation of bubbles and drops under constant pressure conditions, in connection with the Rayleigh-Taylor instability. The validity of that analysis is restrained to interface configurations that admit a simple (one-to-one) projection onto the orifice plane. The purpose of the present paper is to extend the previous theoretical analysis through elementary numerical computations, in order to capture the behaviour of interface profiles, which start from the flat meniscus, and evolve to some undulate structures.

2. Problem formulation

The physical system includes an open cylindrical vessel of quiescent liquid, over a gas chamber. A thin horizontal plate, which is perforated with one small orifice of radius R, separates both fluids. The liquid vessel is assumed large enough, to neglect sidewalls effect, and the free surface. Mathematically, the liquid above the plate extends at infinity. A meniscus forms at the submerged orifice: that meniscus may be flat (the Rayleigh-Taylor case), upward oriented for emerging bubbles, or downward oriented for pendant drops.

The gas pressure p_G is assumed to be constant. The hydrostatic liquid pressure p_L has the particular value p_{L0} over the plate. The equilibrium interface shape depends on R, on the difference between p_G and p_{L0}, on the gravity g, as

well as on the liquid density ρ, and surface tension σ. Two independent dimensionless parameters control this evolution [6], namely the Eötvös number:

$$E\ddot{o} = g\rho R^2/\sigma\,, \tag{1}$$

and the dimensionless excess pressure across the orifice:

$$\Delta = (p_G - p_{L0})R/\sigma\,. \tag{2}$$

The flat meniscus corresponds to $\Delta = 0$, while bubbles and drops are defined by $\Delta > 0$, and $\Delta < 0$ respectively. The cylindrical polar coordinate system (r,θ,z) is defined with $r = 0$ on the orifice axis, and $z = 0$, the horizontal reference plane, at the plate level. The gravity is acting in the negative *z*-direction. A parametric representation of the interface profile is adopted, as $r = r(s,t)$, $z = z(s,t)$, and $\psi = \psi(s,t)$. The curvilinear abscissa *s* is measured, in a meridian plane, from the profile apex $(s = 0)$, to the orifice edge where $s = L$, the maximum arc length. The azimuthal angle ψ defines the unit tangent vector $\boldsymbol{\tau} = (\cos\psi, \sin\psi)$ on the interface. The sense of $\boldsymbol{\tau}$ is such that:

$$r = -\int_0^s \cos\psi \,\mathrm{d}s, \quad z = -\int_0^s \sin\psi \,\mathrm{d}s, \quad \text{and} \quad \boldsymbol{n} = (-\sin\psi, \cos\psi). \tag{3}$$

The unit normal $\boldsymbol{n}$ points outward from the liquid phase.

The appropriate boundary conditions that govern the continuously changing contact line, which is attached at time $t = 0$ to the orifice edge, will be simplified. Adopting a macroscopic point of view, the contact line can be considered as attached to the seemingly sharp edged orifice. All the detailed local physics of contact angles [7] can be by-passed, the studied interface configurations being such that $\theta_r < \psi_c < (\pi + \theta_a)$, where ψ_c is the azimuthal angle at the contact point, θ_r is the limit receding contact angle, and θ_a is the limit advancing contact angle. During the quasi-steady interface evolution, the slow motion in the incompressible inviscid liquid above the interface is supposed to start irrotational and remain so. The velocity potential ϕ satisfies the Laplace equation, $\nabla^2\phi = 0$, and its evolution is governed by the Bernoulli equation:

$$\rho\left(\frac{\partial\phi}{\partial t} + \frac{1}{2}|\nabla\phi|^2\right) + p_L + \rho g\, z = p_{L0}\ . \tag{4}$$

The velocity potential must be finite along the *z*-axis, $\partial\phi/\partial r = 0$, and it vanishes at infinity. There is a vanishing normal velocity at the impermeable plate: $\partial\phi/\partial z = 0$. The normal component of the momentum balance on the interface is written as:

$$p_G - p_L = \sigma(1/R_1 + 1/R_2), \tag{5}$$

where R_1, and R_2 are the local principal radii of curvature. The planar curvature is $1/R_1 = -\mathrm{d}\psi/\mathrm{d}s$. The axisymmetric curvature is $1/R_2 = \sin\psi/r$ outside the axis of symmetry ($r \neq 0$), and it equals the planar curvature on the *Oz*-axis $(r = 0)$.

Combining Bernoulli Equation (4), and momentum balance (5) evaluated at the interface, gives the following equation, written in a dimensionless form:

$$-E\ddot{o}\left(\frac{\partial\phi^*}{\partial t^*} + \frac{1}{2}\left|\nabla^*\phi^*\right|^2\right) = \Delta + E\ddot{o}\, z^* - \left(\frac{1}{R_1^*} + \frac{1}{R_2^*}\right), \tag{6}$$

where the length scale *R*, and velocity scale $U = \sqrt{gR}$ have been adopted. The dimensionless variables have been taken as:

$$z^* = z/R, \quad \phi^* = \phi/(UR), \quad \text{and} \quad t^* = Ut/R. \tag{7}$$

Further, only dimensionless variables will be considered, so to simplify notations, asterisks will be suppressed for convenience in the rest of the paper.

The left-hand side of Equation (6) contains the *transient part*, while the right-hand side contains the *steady part*. The interface equilibrium profile is defined by that steady part:

$$\Delta + E\ddot{o}\, z = 1/R_1 + 1/R_2. \tag{8}$$

The Equation (8) can be rewritten as a coupled set of three first-order ordinary differential equations, by deriving the dimensionless geometric parameters ψ, r and z with respect to the curvilinear abscissa *s*:

$$\begin{cases} \mathrm{d}\psi/\mathrm{d}s = -\Delta - E\ddot{o}\, z + \sin\psi/r, & r \neq 0 \\ \mathrm{d}\psi/\mathrm{d}s = -(\Delta + E\ddot{o}\, z)/2, & r = 0 \\ \mathrm{d}r/\mathrm{d}s = -\cos\psi \\ \mathrm{d}z/\mathrm{d}s = -\sin\psi \end{cases}. \tag{9}$$

The following boundary conditions are available for the interface:

$$\begin{aligned} &\psi(s=0) = \pi, \qquad r(s=0) = 0, \qquad z(s=0) = h \\ &\psi(s=L) = \psi_c, \qquad r(s=L) = 1, \qquad z(s=L) = 0 \end{aligned}. \tag{10}$$

where h denotes the dimensionless profile apex height.

The nonlinear system (9) with boundary conditions (10) is solved numerically as in [8], through a standard shooting method: the integration of the system of ordinary differential equations with initial conditions (imposed values at $s = 0$) is made repetitively by the classical fourth-order Runge-Kutta method, to match the boundary conditions at the edge of the orifice $(s = L)$, via a trial and error process [9]. The apex height h, the maximum arc length *L*, and the azimuthal angle at the orifice edge ψ_c are obtained upon the numerical integration of the above system. For a given pair of control parameters $\{E\ddot{o}, \Delta\}$,

we found several equilibrium interface profiles, which correspond to different h-values (implicitly to different values of L and ψ_c). For drops, the numerical procedure follows that of bubbles, with some differences: $h<0$, the last equation in (9) changes its sign, and $\psi(s=0)=0$ in (10).

3. Bifurcating solutions

Within the stability analysis performed by Achard and Georgescu [6], the interface profile magnitude is expressed by the amplitude ε (positive for bubbles, and negative for drops), defined as:

$$\varepsilon=\sqrt{2}\int_0^1 r\tilde{\xi}(r)\frac{J_0(\lambda_1 r)}{J_1(\lambda_1)}\,\mathrm{d}r\,, \tag{11}$$

where $\lambda_1=2.40482556$. The Equation (11) includes the steady solution $\tilde{\xi}$ of the interface representation $z=\xi(r,t)=\tilde{\xi}(r)+\hat{\xi}(r,t)$, which defines only profiles that admit a simple projection onto the orifice plane. It follows that the apex height is then: $h=\tilde{\xi}(0)$. For small axial disturbances $\hat{\xi}$ about $\tilde{\xi}$ at $\Delta=0$, the stability of the null solution $\tilde{\xi}=0$ (that is the flat meniscus) has been tested in [6, Section 4], together with the stability of the bifurcating solutions, $\tilde{\xi}>0$ for bubbles, and $\tilde{\xi}<0$ for drops [6, Sections 5-6]. The general condition for loss of stability has been described for the flat meniscus, $\tilde{\xi}=0$, by two eigenvalues:

$$\sigma^{(1)}(\mu)=\pm\sqrt{\mu/m_1}\,, \tag{12}$$

where $m_1=\left(Eö\left[J_1(\lambda_1)\right]^2\right)/2$ is the added mass coefficient, and μ is defined as:

$$\mu=Eö-\lambda_1^2=Eö-5.783186\,. \tag{13}$$

The flat meniscus is thus stable when $\mu<0$ (that is when $Eö<5.783186$), and unstable when $\mu\geq 0$. In the neighbourhood of $\varepsilon=0$, the subcritical bifurcation diagram (in the plane $\Delta=0$) has been analytically defined by [6, Equation (49)]:

$$\mu=-36.73425\,\varepsilon^2\,. \tag{14}$$

Its upper branch ($\varepsilon>0$) corresponds to bubbles, while its lower one ($\varepsilon<0$) corresponds to drops. Those two branches emerge symmetrically from the critical point P_1, situated at $\mu=0$ (that is $Eö=5.783186$), $\Delta=0$, and $\varepsilon=0$. For $\Delta=0$, it was shown that the solution $\tilde{\xi}\neq 0$ is unstable as it bifurcates at the critical point [6, Section 6]. In Figure 1 we plot the bifurcation diagram in the plane ($Eö$,ε). The analytical curve of Equation (14) is transformed as $Eö=Eö(\varepsilon)$ due to Equation (13). In Fig. 1 we also plot numerical results obtained within this paper from Equations (9-10), and transformed then in terms of ε through Eq. (11).

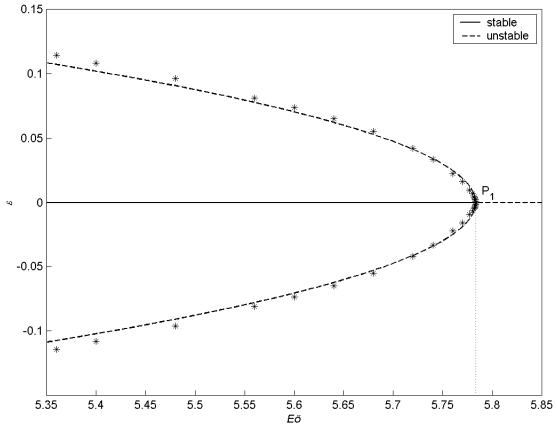

Fig. 1. Subcritical bifurcation diagram $(\Delta = 0)$: analytical curves, together with numerical results plotted by star marks. Stable parts are plotted in solid line, while unstable parts are dashed

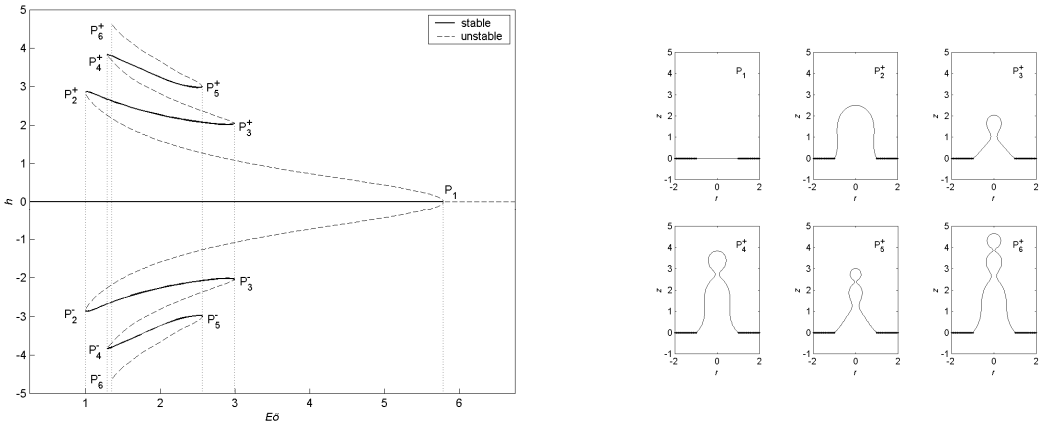

Fig. 2. Left: complete bifurcation diagram obtained numerically $(\Delta = 0)$. Stable parts are plotted in solid line, while unstable parts are dashed. Right: typical profiles of bubbles in P_2^+ $(Eö = 0.996)$, P_3^+ $(Eö = 2.990)$, P_4^+ $(Eö = 1.286)$, P_5^+ $(Eö = 2.560)$, P_6^+ $(Eö = 1.348)$, and the flat meniscus in P_1 $(Eö = 5.783186)$

We extend here the above stability analysis far from the flat meniscus, to interface configurations that have an undulate structure (with one, or two necks). The parametric representation is convenient. The representative interface magnitude in the present paper is the apex height *h* (positive for bubbles, and negative for drops), which results upon numerical integration of Equations (9-10).

In Figure 2, we present the complete bifurcation diagram (in the plane $\Delta = 0$), obtained numerically far from $h = 0$. Various turning points have been identified, being denoted $P_2^+, P_3^+, \ldots, P_5^+, \ldots$ when referring to bubbles, and $P_2^-, P_3^-, \ldots, P_5^-, \ldots$ when referring to drops. Typical profiles are plotted for bubbles corresponding to the turning points $P_2^+, \ldots, P_6^+$, together with the critical flat meniscus situated in P_1. The drops profiles at $P_2^-, \ldots, P_6^-$ are just symmetrical to the corresponding bubble profiles, with respect to the orifice. The stability of the bifurcating solutions far from the flat meniscus will be discussed upon an extended eigenvalue problem [6, Equation (53)], modified here by introducing the representation $r = \eta(z,t)$ for necking interfaces (within the analytical study, the parametric representation is not convenient). The dependant variable varies between 0 and h. The apex height must be immobilized by introducing a change of coordinates. Nevertheless the resulting eigenvalue problem has the same structure as [6, Eq. (53)], and proceeding formally by using the *Factorisation Theorem* proposed by Iooss and Joseph [10], we also find two eigenvalues:

$$\sigma^{(1)}(h) = \pm\sqrt{\mu_h(h)/M(h)}\,, \tag{15}$$

where $M(h) > 1$ is proportional to the added mass of the liquid. Note that $\sigma^{(1)}(h)$ as given by Equation (15) is not symmetric in h due to $M(h)$, the added mass effects being different for bubbles and drops. Thus, starting from the critical flat profile, the equilibrium bubble and drop configurations at $\Delta = 0$ are unstable before reaching the left-hand side turning points, and stable after that. The reverse is true on the right-hand side turning points. In the typical one-sided subcritical bifurcation plotted in Figure 2, the turning points limit thus zones where stable bubbles, or drops should be observed. Profiles have one neck on the stable branches $\{P_2^+, P_3^+\}$ and $\{P_2^-, P_3^-\}$, and two necks on the stable branches $\{P_4^+, P_5^+\}$ and $\{P_4^-, P_5^-\}$.

4. Isolated solutions that break bifurcation

For small axial disturbances $\hat{\xi}$ about $\tilde{\xi}$ at $\Delta \neq 0$, the stability of isolated solutions $\tilde{\xi} \neq 0$ has been analysed in [6, Section 7], near the critical point P_1. In the space $(\mu, \Delta, \varepsilon)$, steady solutions $\tilde{\xi}$ define an equilibrium surface, which is a *cusp* described analytically by [6, Equation (79)]:

$$\Delta(\mu, \varepsilon) = -1.70046\,\mu\varepsilon - 62.46528\,\varepsilon^3\,. \tag{16}$$

The upper cusp sheet corresponds to bubbles, and the lower one corresponds to drops. The turning points P_1^+ and P_1^- extend into $\Delta > 0$, and $\Delta < 0$ regions as

singularity lines (fold curves) of that cusp. The intermediate sheet of the cusp, which is bordered by P_1^+ and P_1^- singularity lines, is stable. The upper and lower sheets of the cusp (that is above P_1^+, and below P_1^- lines) are unstable. Those singularity lines are defined by the following system [6, Equation (81)]:

$$\begin{cases} \Delta = 124.93056\,\varepsilon^3 \\ \mu = -110.20302\,\varepsilon^2 \end{cases}, \tag{17}$$

and represent the analytical bifurcation curve near the critical point. Upon combining Equations (13) and (17), the analytical bifurcation curve is plotted in Figure 3 onto the control parameter plane (*Eö*,*Δ*), together with the numerical results obtained in this paper through Equations (9-11). Far from the critical point P_1, the equilibrium surface can be found via the numerical approach.

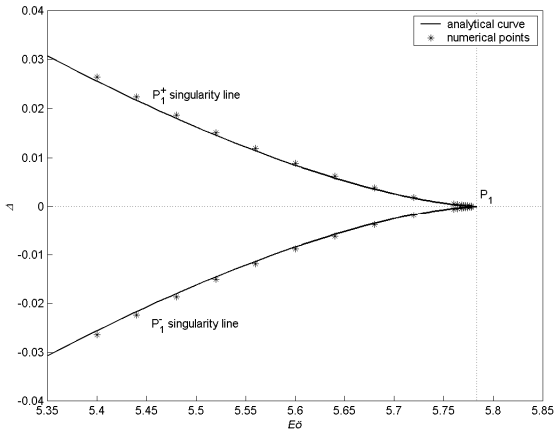

Fig. 3. Analytical (solid line), and numerical (star marks) bifurcation set near the critical point P_1. The upper branch is the projection of the P_1^+ singularity line of the bubbles cusp sheet onto the plane (*Eö*,*Δ*); the lower branch is the projection of the P_1^- singularity line of the drops cusp sheet

Equations (9-10) give the steady interface profiles that correspond to each point of the equilibrium surface in the whole space (*Eö*,*Δ*,*h*). The equilibrium surface is very complex at very low Eötvös numbers, say $Eö < 0.045$, as well as at large *Eö*, say $Eö > 6.5$. We will restrict our numerical investigation mainly between these limits, which cover a very large spectrum of physically interesting cases. The 3D shape of the equilibrium surface is difficult to be plotted entirely: it is a cusp at low *h*-values, and it becomes multifold when increasing apex height (the surface zigzags away from the $h = 0$ plane, and is antisymmetric in Δ); at high apex height values, the multifold surface exhibits even a sequence of swallowtails. The equilibrium surface intersects the plane $\Delta = 0$ according to the

curve given in Figure 2. The turning points P_j^+ $(j = 2,\ldots,6)$ for bubbles, and their counterparts P_j^- for drops, form singularity lines (fold curves) when extending into $\Delta > 0$, and $\Delta < 0$ regions of the space (*Eö*,*Δ*,*h*); those fold curves will be denoted by the same symbols as their turning points, i.e. P_j^+ and P_j^-.

To understand better the configuration of the equilibrium surface, we plot in Figure 4 complete cross sections of the equilibrium surface, for some typical *Eö*-values. For $Eö = 2.8$, a cross section of the 3D surface restricted mainly to the upper (bubble) part, is plotted in Figure 5, together with some typical stable configurations of the interface profiles, at the same *Δ*-value (i.e., $\Delta = -0.4$).

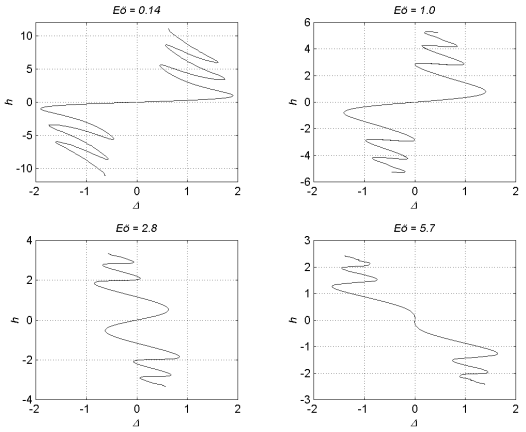

Fig. 4. Dependence $h = h(\Delta)$ for bubbles and drops, at: $Eö = 0.14$ (upper left); $Eö = 1.0$ (upper right); $Eö = 2.8$ (lower left); $Eö = 5.7$ (lower right)

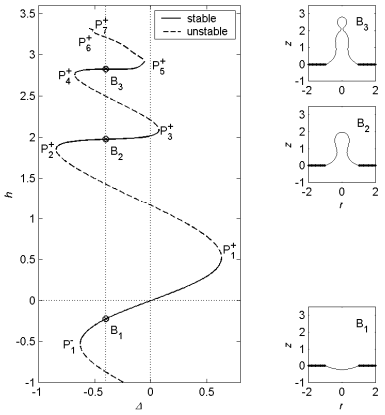

Fig. 5. Dependence $h = h(\Delta)$ for $Eö = 2.8$, restricted mainly to the bubbles part (left); typical stable profile configurations for $\Delta = -0.4$, at B_1 (drop), B_2 & B_3 (bubbles)

For bubbles, the singularity lines P_j^+ $(j = 1,\ldots,4)$ are projected onto the control parameter plane (*Eö*,*Δ*) in Figure 6. The singularity lines P_j^- for drops are also drawn in this figure; they are symmetrical to P_j^+ with respect to the $\Delta = 0$ plane. For j up to 4, the fold curves are roughly parallel, so a 3D graphical representation can be plotted. Consider firstly the cusp that straddles on the flat meniscus. The bifurcation curve, which is the projection of the first singularity lines P_1^+ and P_1^- onto the plane (*Eö*,*Δ*), follows the path of numerical star marks plotted in Fig. 3. The upper cusp sheet, and the lower one are bordered by the

second singularity lines, defined by the turning points P_2^+ and P_2^-. Over the entire cusp surface, interface profiles are not necked. In Figure 7 (left), we plot the cusp that we computed numerically, together with the bifurcation curve. Consider next the multifold part of the equilibrium surface. It is plotted in Fig. 7 (right side), for a restrained *Eö* range, starting from the flat meniscus up to the fifth fold curve.

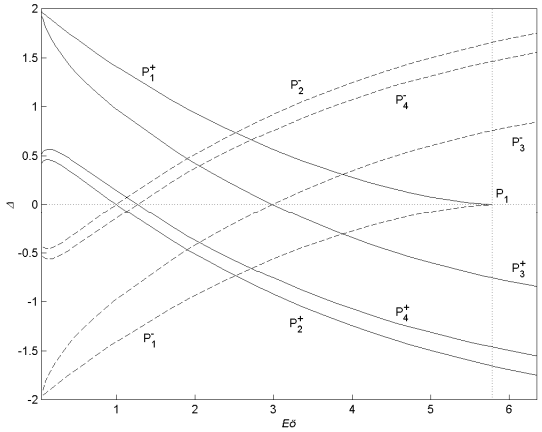

Fig. 6. Bifurcation set: singularity lines P_j^+ for bubbles (solid lines) and P_j^- for drops (dashed lines), for $(j=1,\ldots,4)$, projected onto the control parameter plane (*Eö*,*Δ*); $Eö \in [0.045, 6.5]$

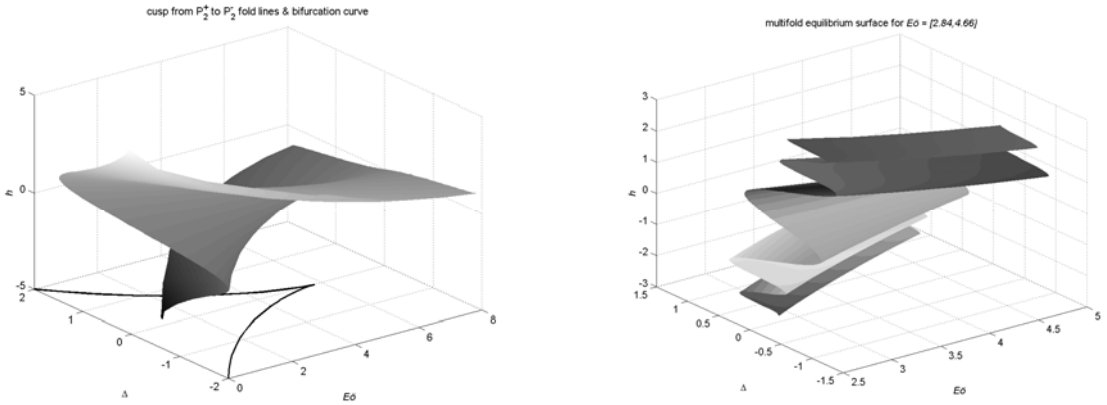

Fig. 7. Left: equilibrium surface between P_2^+ and P_2^-, and bifurcation curve. Numerical computations for that cusp correspond to $Eö \in [0.4, 8.0]$; Right: multifold equilibrium surface for $Eö \in [2.84, 4.66]$

The stability study of isolated solutions $(\Delta \neq 0)$, which perturb bifurcating solutions $(\Delta = 0)$, will be based on the stability study of the latter, presented in [6, Section 6]. The relations $\mu = \mu(\varepsilon)$, and $\tilde{\xi} = \tilde{\xi}(\varepsilon)$ for $\Delta = 0$ will be replaced by the relations $\Delta = \Delta(\mu, \varepsilon)$, and $\tilde{\xi} = \tilde{\xi}(\mu, \varepsilon)$, in which μ is a fixed parameter such as $\mu < 0$. Far from the critical point, the solution magnitude is represented by the apex height h, and the Equation (15) has the following analogue:

$$\sigma^{(1)}(\mu, h) = \pm\sqrt{\Delta_h(\mu, h)/M(\mu, h)}, \tag{18}$$

where $\Delta_h(\mu, h)$ changes the sign as h is varied at each regular turning point. Likewise in Section 3, at each turning point, the sign of $\Delta_h(\mu, h)$ controls whether $\sigma^{(1)}$ is a couple of real, or purely imaginary eigenvalues. The stability properties of that *imperfect problem* $(\Delta \neq 0)$ are consistent with those found for the *perfect problem* $(\Delta = 0)$ treated in Section 3.

Consider the cross section of the equilibrium surface (*Eö*,*Δ*,*h*) presented in Figure 5. The first sheet $\{P_1^-, P_1^+\}$ that crosses the *Eö*-axis is stable (solid line in Figure 5), since precisely this axis has been found to be stable for the flat meniscus case (Rayleigh-Taylor problem), as soon as $Eö < 5.783186$ [6, Section 4]. The next sheet, *e.g.* $\{P_1^+, P_2^+\}$ for bubbles, is thus unstable (dashed line in Figure 5). Observe that it crosses the $\Delta = 0$ plane according to a curve that has already been shown to be unstable in the perfect case (line $\{P_1, P_2^+\}$ in Figure 2). The further sheet $\{P_2^+, P_3^+\}$ is stable and so on, up to the 6th sheet $\{P_5^+, P_6^+\}$, which is unstable. Each time when crossing $\Delta = 0$, we found results consistent with those obtained in Section 3. For the particular value of $Eö = 2.8$, note that the 5th sheet no longer crosses the plane $\Delta = 0$. To sum up, pieces of surfaces delimited by the couples of fold curves $\{P_1^-, P_1^+\}$, $\{P_2^+, P_3^+\}$, $\{P_4^+, P_5^+\}$, as well as by $\{P_2^-, P_3^-\}$, $\{P_4^-, P_5^-\}$, correspond to stable bubbles, or drops configurations. Only bubbles and drops corresponding to $\{P_1^-, P_1^+\}$ seem to have been currently observed. Bubbles and drops corresponding to $\{P_2^+, P_3^+\}$, and $\{P_2^-, P_3^-\}$ are single necked; they appear less common. Profile configurations of $\{P_4^+, P_5^+\}$, and $\{P_4^-, P_5^-\}$ have two necks; they haven't been observed. The reason may be that it is difficult to control formation of bubbles and drops close enough to these solutions. For $Eö < 5.783186$, when interfaces are strongly disturbed to make them escape from the attraction set of the flat meniscus, they grow into bubbles or drops, without being stopped by the nearest unstable sheet. So they absorb more

and more transient effects, and the following stable sheet cannot attract and stabilise them. Another reason is that the projection of these pieces of surface on the plane (*Eö*,*Δ*), as seen in the bifurcation set of Figure 6, corresponds to stripes that become narrow as the apex height grows. Thus, *Δ* must be carefully tuned to attain say the $\{P_2^+, P_3^+\}$ sheet, for a given *Eö*.

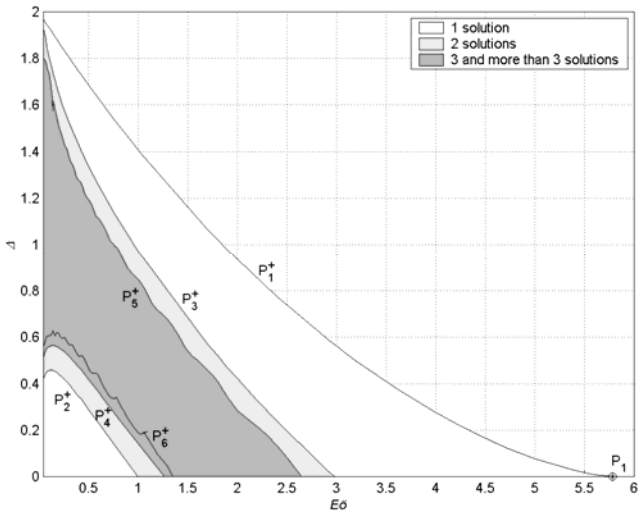

Fig. 8. Number of stable solutions in regions bordered by the projection of singularity lines P_j^+ $(j = 1,\ldots,6)$ onto the control parameter plane (*Eö*,*Δ*), for $\Delta > 0$

Far from P_1, projections of fold curves corresponding to P_j^+ $(j = 1,\ldots,6)$ have been plotted in Figure 8, for $\Delta > 0$. In each region bordered by these curves projections, the number of stable solutions is indicated. For $j \le 4$, this figure may be compared to Figure 6 (where P_5^+, and P_6^+ do not appear). For $j > 4$, the fold curves are no longer smooth: they are distorted, and even exhibit *swallowtails*, which are singularities well known in the Catastrophe Theory. A particular sequence of such singularities is presented in Figure 9, together with typical bubble profiles around a selected swallowtail [8; 11]. At high apex height values, corresponding to fold curves P_5^+, and P_6^+, as well as to swallowtails, bubbles and drops have an undulate structure with two necks. Around a selected swallowtail, at constant *Eö*, we did not find significant differences between bubble profiles for quite small changes in *Δ*-values (this last observation is valid for drops too). On the left side, and on the right side of a swallowtail, the apex height has different sense of variation when *Δ*-values increase monotonously. In fact, the upper branch

of the swallowtail corresponds to the seventh turning point P_7^+ (see the bubble index *s*7, or *m*7 in Figure 9). Usually, the 7th turning point follows closer the 6th one (*e.g*. in Figure 5). The lower left branch of the swallowtail corresponds to P_6^+ (see the bubble index *s*6, or *m*6 in Figure 9), and the lower right branch corresponds to P_8^+ (see *s*8, or *m*8 in Figure 9). Because of the complexity of the whole sequence of turning points, which appear and disappear at high *h*-values, when increasing *Eö*, we denoted the whole distorted 6th fold line with its swallowtails as the P_6^+ fold line. The same apply for denoting the distorted P_5^+ line, where at lower *Eö*, some swallowtails also appear.

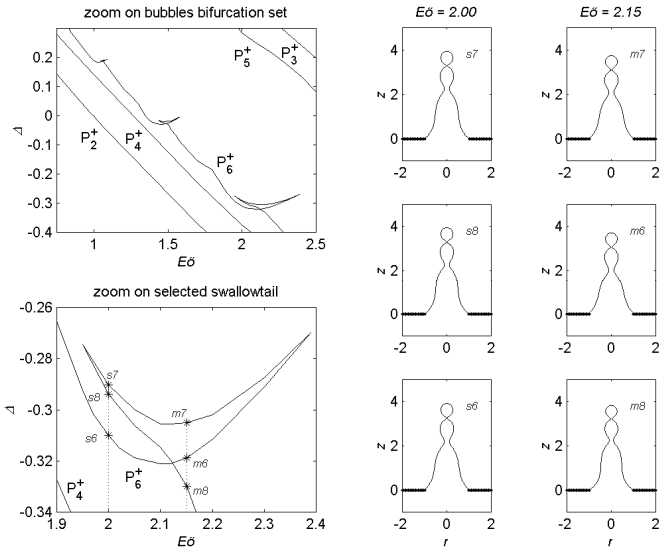

Fig. 9. Left: zoomed bifurcation set for bubbles (upper left), showing a sequence of swallowtails on P_6^+ singularity line, for $Eö \in [0.75,2.5]$, and $\Delta \in [-0.4,0.3]$; selected swallowtail (lower left) within the ranges $Eö \in [1.9,2.4]$, and $\Delta \in [-0.34,-0.26]$ (star marks show the position of 3 profiles at $Eö = 2$, and $Eö = 2.15$); Right: bubble profiles around the selected swallowtail, for $Eö = 2$, where $h|_{s6} < h|_{s7} < h|_{s8}$, and for $Eö = 2.15$, where $h|_{m6} < h|_{m7} < h|_{m8}$

As stated before, stable undulate (necked) structure of bubbles and drops were not observed so far in Newtonian liquids. Anyhow, as mentioned in Introduction, Kliakhandler reported in [4] that undulate bubble structures may be found in concentrated polymeric solutions. To investigate qualitatively the existence of such necked bubbles, following [4], some simple experiments were

conducted [12]: we present in Figure 10 the experimental results corresponding to stable multi-necked bubbles in a polymeric solution, with density of $900\,\mathrm{kg/m^3}$, surface tension of $0.0225\,\mathrm{N/m}$, zero shear viscosity of $7.5\,\mathrm{Pa\cdot s}$, and time of relaxation of $0.3\,\mathrm{s}$, at 20°C. The polymeric solution filled a transparent cylinder of 65 mm diameter, open at its upper part. Obviously, due to the liquid elasticity, stable undulate interface configurations can be easily found. It must be highlighted that the bubbling we performed experimentally, as Kliakhandler does [4], corresponds to bubbles attached to a nozzle, the air being injected slowly, under constant flow conditions (we used a nozzle with inner radius of 0.45 mm). Our numerical study deals with constant pressure conditions. We mention that the evolution of the necked interface in polymeric solution is such that some bubbles are *breathing* through their necks (see the two successive sequences from the left in Figure 10): the air is supplied through each neck, producing the alternative growth, and reduction of each volume that exists between two necks. Obviously, the elastic properties are preventing the complete necking of the interface, and the bubble detachment. Anyhow, those experimental results allow doing some qualitative comparison: the sequence we cut from the undulate bubble in the right side of Figure 10, is more like the bubbles we found numerically for P_6^+ (Figures 2 and 9).

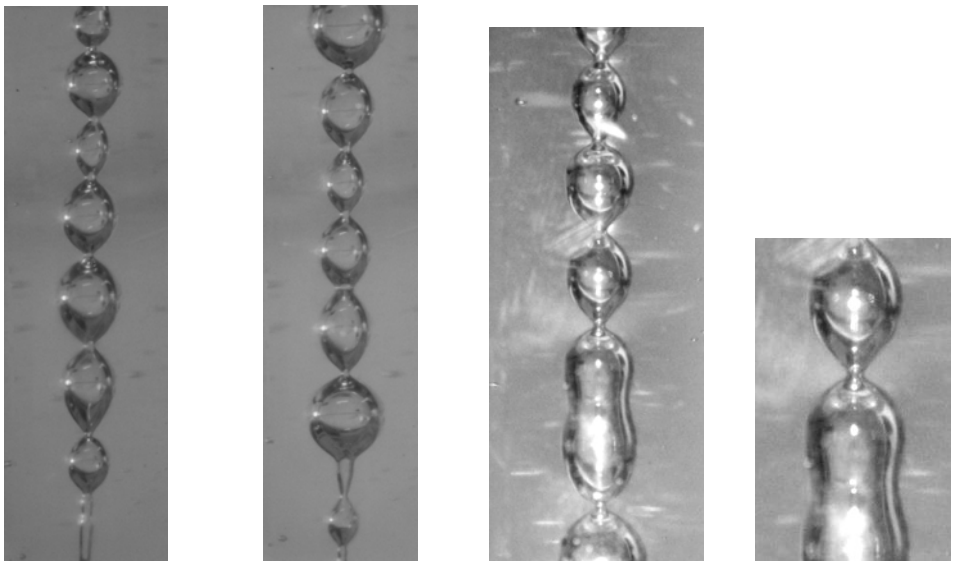

Fig. 10. Undulate bubble structures in polymeric solution, at $Eö = 0.079$ [12]. Left: two successive sequences of the necked interface evolution; each bar is 65 mm height. Right: a particular necked interface shape, and its zoomed cutting sequence

5. Conclusions

The stability analysis performed in [6] has brought a unified picture of the quasi-steady formation of bubbles and drops at a submerged orifice, under constant pressure conditions, in connection with the Rayleigh-Taylor instability. This analytical analysis is valid only near the critical point P_1 of the flat meniscus, where the Eötvös number has the particular value $Eö = 5.783186$, and the excess pressure number is $\Delta = 0$ (Δ includes the pressure difference between gas and liquid across the orifice). In the present paper, the above stability analysis has been extended far from P_1, through elementary numerical computations.

For the interface profiles (bubbles, drops), bifurcating steady solutions (corresponding to $\Delta = 0$), together with isolated solutions ($\Delta \neq 0$) that perturb the former-ones, are provided numerically for a wide range of the control parameters ($Eö$,Δ), by taking the apex height h as the profile magnitude (positive for bubbles, and negative for drops). It is shown that h zigzags away from the $h = 0$ axis, being antisymmetric in Δ; at each turning point (P_j^+ for bubbles, and P_j^- for drops, with $j \geq 1$), solutions change their stability characteristics.

An explicit picture of the equilibrium surface has been given in [6] near the critical point. It corresponds to a *cusp*, whose intermediate sheet is stable, while its two upper and lower sheets are unstable. The bubbles and drops configurations corresponding to that cusp are not necked; the profiles onto the intermediate sheet of the cusp are the ones that are usually observed. Numerical computations provide the complete equilibrium surface in terms of h for the global variation in the controls $(Eö, \Delta)$, over the half plane $Eö > 0$. In this three-dimensional space, the equilibrium surface is multifold in both Δ directions.

In fact, the turning points P_j^+ and P_j^- extend into $\Delta > 0$, and $\Delta < 0$ regions as singularity lines (fold curves), which stay roughly parallel for $j \leq 4$ in the selected range $Eö \in [0.045, 6.5]$. For $j > 4$, the fold curves are distorted and exhibit *swallowtails*. The fold curves P_j^+ and P_j^- border superimposed stripes of the equilibrium surface, where solutions are alternatively stable, and unstable. For instance, the surface stripes bordered by the couple of fold curves $\{\mathrm{P}_2^+, \mathrm{P}_3^+\}$, and $\{\mathrm{P}_2^-, \mathrm{P}_3^-\}$ correspond to stable bubble, and drops configurations, which have one neck. On the stripes bordered by $\{\mathrm{P}_4^+, \mathrm{P}_5^+\}$, and $\{\mathrm{P}_4^-, \mathrm{P}_5^-\}$, stable bubbles, and drops have two necks. The experimental study of those stable configurations deserves some attention, since the corresponding undulate profiles have not been observed so far in Newtonian liquids. Following Kliakhandler [4], it was shown experimentally within this paper that stable undulate bubble configurations might

exist in concentrated polymeric solutions, due to the liquid elasticity. Anyhow, to validate our theoretical results, new designed experiments using highly viscous Newtonian liquids are necessary, attempting to damp perturbations, and to obtain stable profiles. Perhaps most experiments fall out of the restricted range of parameters insuring the existence of a stable solution, as indicated in the bifurcation set (Figure 8).

REFERENCES

[1]. *S. S. Sadhal, P. S. Ayyaswamy and J. N. Chung*, Transport Phenomena with Drops and Bubbles, Springer, New-York, 1997

[2]. *H. Tsuge*, "Hydrodynamic of bubble formation from submerged orifices", in Encyclopedia of Fluid Mechanics, N. P. Cheremisinoff (ed.), Gulf Publishing, Houston, 1986, pp. 191-232

[3]. *J. F. Padday*, "Transient surface properties in liquid bridge and pendant drop menisci in gravity and low gravity", in Dynamics of Multiphase Flows across Interfaces, Lecture notes in Physics, A. Steichen (ed.), Springer, Berlin, 1996, pp. 41-55

[4]. *I. Kliakhandler*, "Continuous chain of bubbles in concentrated polymeric solutions", in Phys. Fluids, **vol. 14**, no. 10, 2002, pp. 3375-3379

[5]. *J. Pakleza, J.-B. Chalfen, M.-C. Duluc, T. Kowalewski and A. Cybulski*, "Méthodologie expérimentale pour l'étude de la croissance de bulles de vapeur en site isolé", in Actes du Congrès Français de Thermique, SFT 2001, Nantes, France, 2001, pp. 467-472

[6]. *J.-L. Achard and Sanda-Carmen Georgescu*, "Quasi-steady formation of bubbles and drops viewed as processes that break bifurcation", in Journal of Engineering Mathematics, **vol. 52**, 2005, pp. 147-164.

[7]. *A. Marmur and E. Rubin*, "Equilibrium shapes and quasi-static formation of bubbles at submerged orifice", in Chem. Engng Sci., **vol. 28**, 1973, pp. 1455-1464

[8]. *Sanda-Carmen Georgescu*, Évolution d'une bulle: Formation à partir d'un orifice et éclatement à la traversée d'une surface libre, PhD Thesis, Institut National Polytechnique de Grenoble, France, 1999

[9]. *W. H. Press, S. A. Teukolsky, W. T. Vetterling and B. P. Flannery*, Numerical Recipes in FORTRAN: The Art of Scientific Computing, 2nd edition, Cambridge University Press, Cambridge, 1992

[10]. *G. Iooss and D. D. Joseph*, Elementary Stability and Bifurcation Theory, 2nd edition, Springer, New-York, 1990

[11]. *Sanda-Carmen Georgescu and J.-L. Achard*, "Profile singularities appearing during the quasi-steady formation of bubbles and drops at constant pressure", in: Numerical Methods in Fluid Mechanics and Fluent Applications, I. Anton R. Resiga, V. Sofonea, S. Bernad and S. Muntean (eds), Editura Orizonturi Universitare, Timişoara, Romania, 2003, pp 113-120

[12]. *Sanda-Carmen Georgescu, T. Muntean, C. Bălan, F. I. Ioana and I. Deaconu*, "Experimental visualisation of slow bubbles formation in highly viscous fluids" (in Romanian), in Proc. 3rd National Conference "Dorin Pavel", Bucharest, 2004, pp 93-100.